Effect of Post-Weld Heat-Treatment on Corrosion and Microstructure Properties of Electric Arc Welded Mild Steels*

O. O. Ajide[1], O. O. Anifalaje[1], I. G. Akande[1, 2**], F. A. Musa[1], O. S. I. Fayomi[2, 5], O. O. Oluwole[1], K. M. Oluwasegun[3] and O. J. Ajao[4]

[1]*Department of Mechanical Engineering, University, Ibadan, Oyo State, Nigeria*
[2]*Department of Mechanical Engineering, Bells University of Technology, P.M.B. 1015,Ota, Ogun State, Nigeria*
[3]*Department of Mechanical Engineering, University of Manitoba, Winnipeg, Manitoba, Canada*
[4]*Department of Mechanical Engineering, Howard University, Washington, D.C., USA*
[5]*Faculty of Engineering and Built Environment, University of Johannesburg, Auckland Park, P. O. Box 534, Johannesburg, South Africa*

**Corresponding author: aigodwin2015@gmail.com

Abstract

Welding has been an incredibly important process used to join metals in several industrial applications, such as manufacturing, construction, automotive and aerospace sectors. It has been reported that welded joints sometimes exhibit poor corrosion resistance, due to the changes in the weld surface or HAZ chemical composition, residual stress and metallurgical structure. Therefore, there is a need to enhance welds corrosion resistance and microstructure properties through PWHT. In this study, PWHTs effect on the corrosion and microstructure properties of two MSs, SAE 1015 and 1010, which were fused by electric metal arc welding, was examined. The MS samples, with different chemical compositions, were cut to the desired dimensions, separately welded and, thereafter, subjected to PWHT, at 650, 750, 850 and 950 ºC, for 1 h. The corrosion and microstructure properties of the PWHT MS samples immersed in 3.5 wt.% NaCl were then investigated, using PDP and SEM, respectively. For the PWHT SAE 1015 and 1010 MS samples, the lowest CR values were 34.240 and 35.793 mm/year, at 650 ºC, while the highest were 90.16 and 60.10 mm/year, at 950 ºC, respectively. For the AW SAE 1015 and 1010 MS samples, the CR values were 107.54 and 118.09 mm/year, respectively. The SEM images revealed smaller grain sizes and boundaries and less porosity for PWHT MS samples at 650 ºC than for those at 950 ºC. Therefore, the first ones are recommended for advanced industrial applications.

Keywords: AW MS**,** corrosion, microstructure, MS SAE 1015 and 1010, PWHT and welding.

Introduction

Over the years, different types of materials have been used by industries, for several applications. Among them, steel is one of the most widely used, due to its low cost and ready availability [1-3]. Steel has been used in many industrial applications that

---

* The abbreviations list is in page 54.

involve high strain rates and stresses [4, 5]. Low and medium C steels are essential engineering materials, which have found different applications in marine applications, transportation and chemical processing, due to their availability, low cost, good mechanical properties, ease of fabrication and weldability [6, 7]. These steels account for a large percentage of all annual steel production and availability all over the world [8, 9]. Steel has also been employed for railway, coupling, driving rings, flanges, hand tools, sockets, levers, cams, machinery parts, such as nuts and bolts, shafts and gears, connecting rods and laminated springs. These numerous applications have made essential the study of steel welded joints mechanical, corrosion and microstructural properties.

Welding is an amazingly significant industrial process that is used in automotive industries, high rise office buildings, aeroplanes, rockets and pipelines. More specifically, arc welding is the most common type of welding, whereby the source of heat is supplied by a high-current electric arc, between the base metal and the electrode material [10, 11]. The generated heat is enough to melt the electrode tip and the base metal. Due to this large amount of generated heat, the base metals melt, and a strong welded joint is formed after its cooling.

It has been discovered, in most cases, that welded joints exhibit lower resistance to corrosion and weaker mechanical properties, since welding causes changes in their chemical compositions, residual stress and structure [12, 13], which could make the soldered metal and the HAZ corrode more rapidly than the base metal [14-16].

Corrosion failure, which can cause welds mechanical and microstructural failures, often occurs, in spite of the selection of suitable base and filler metals, and strict adherence to industry codes and standards. There are also instances in which the weld exhibits higher corrosion susceptibility than that of the unwelded base metal [17].

However, with HT aid, these problems can be mitigated. PWHT has been reportedly employed, in order to reduce the residual stress gradients, and also to minimize the welded joint susceptibility to stress corrosion cracking [18-20]. PWHT minimizes the composition gradients and the formation of micro galvanic cells. This treatment also transports hydrogen from the weld regions, thus preventing its cracking or embrittlement [21, 22]. In this study, suitable HT conditions for enhancing electrochemical corrosion and microstructural characteristics of two PWHT MS grades were investigated.

Materials and methods

The investigated MS plates (base metals) chemical compositions were determined by OES (Table 1).

Table 1. MS samples chemical compositions (% mass).

Steel	Fe	C	Cr	S	P	Mn	Mo	Ni	Si
SAE 1015	99.232	0.150	0.004	0.003	0.005	0.539	0.005	0.035	0.027
SAE 1010	99.322	0.100	0.002	0.003	0.005	0.534	0.005	0.004	0.025

A Hero E6013 Stone bridge flux coated MS electrode was used to supply the filler metal. The flux (a thin layer coating around the welding electrode) provided a shield to the molten metal zone from the atmospheric O and N during welding. This flux

also prevented the formation of O^{-2} and N^{-3}. The flux chemically reacted with O^{-2} in the metal, forming a low melting temperature fusible slag. The used electrodes diameter and length was 2.5 and 300 mm, respectively. The MS electrode chemical composition is shown in Table 2.

Table 2. MS electrode chemical composition (% mass).

Electrode	C	Mn	Si	S	P
MS	0.12	0.50	0.33	0.031	0.040

Electric arc welding procedure

Electric arc welding was performed on the base metals using an AC electric machine. The base metals were thoroughly cleaned with a wire brush, in order to remove impurities and corrosion products that could lead to weak welds or porous welded surfaces. The MS electrode was inserted into the electrode holder, at an angle of 60 to 80°, with the work piece placed in Fig. 1. The welding procedure was done by bringing the electrode in contact with the base metals, and then separating the former to a proper distance, in order to produce an arc. When the arc was obtained, the intense heat melted the base metals below the arc, thus forming a molten metal pool. A small depression was formed in the base metals, and the molten metal, called arc crater [23, 24], deposited around the edge of this depression. The weld beads length was about 40 mm each, and the weldments width was approxim. 10 mm. After welding, the specimens were naturally cooled to room temperature, in still air. The slag that floated on top of the weld was brushed off after solidification and cooling of the weld joint.

Figure 1. Base metal samples joining by electric arc welding process.

PWHT and sample preparation

After welding, the samples were subjected to PWHT, with a holding time of 1 h each, and at soaking temperatures of 650, 750, 850 and 950 ºC, using a Lenton electric furnace, in order to compensate for the joints properties weakening caused by the unequal volume fractions of ferrite and austenite in the weld zone. Then, the samples were cooled to room temperature in still air, polished, rinsed in distilled water, and cut into 10 x 10 x 5 mm, for various examinations.

Corrosion testing

These MS samples were mounted on a Cu wire, and then embedded in epoxy resin for the corrosion test, using PDP technique in a three-electrode cell. 100 mL seawater (3.5 wt.% NaCl) were used as the corrosion medium, at the room temperature of 25 ºC. The WE, RE and CE were inserted in the test

solution. The MS weld, the graphite rod and the saturated calomel acted as WE, CE and RE, respectively. The polarization was performed at a SR of 0.166 mV/s, from -250 mV OCP to +1000 mV of SCE. The CR was calculated using equation 1.

$$\text{Corrosion rate (mm/year)} = \frac{0.00327 \times \text{jcorr} \times \text{EW}}{\text{D}} \tag{1}$$

where j_{corr} is the corrosion current density (A/cm^2), EW is the equivalent weight (g) and D is the metal density (g/cm^3). By the Tafel extrapolation, the j_{corr} was determined.

Microstructural examination
SAE 1015 and 1010 MS samples microstructural examination was carried out using a SEM at the magnification of 250X.

Results and discussion
Corrosion properties
Table 3, Figs. 2 and 3 illustrate the effect of 3.5 wt.% NaCl on AW and PWHT SAE 1015 MS samples.

Table 3. Polarization data for AW and PWHT SAE 1015 MS samples.

Temp.	E_{corr} (V)	j_{corr} (A/cm^2)	CR (mm/year)	R_p (Ω)
AW	-0.6216	0.009255	107.54	4.1925
PWHT at 650 ºC	-1.1615	0.002947	34.24	24.550
PWHT at 750 ºC	-1.1614	0.003198	37.16	17.347
PWHT at 850 ºC	-1.1411	0.003629	42.17	34.020
PWHT at 950 ºC	-1.1764	0.007759	90.16	15.899
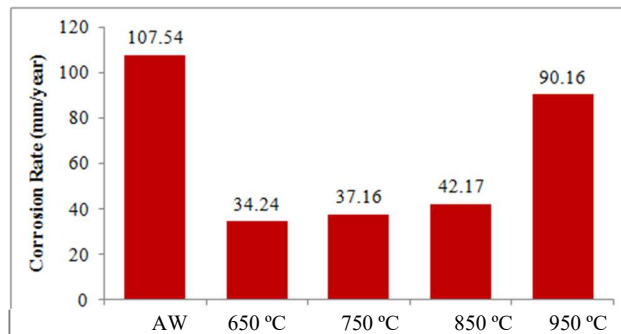
Figure 2. CR values of AW and PWHT SAE 1015 MS samples, at different temperatures.

Table 3 shows that the PWHT MS sample had lower corrosion j_{corr} values than those from the AW sample, which could be attributed to the HT effect that minimized the ions exchange within the metal anodic and cathodic sites. At 650 ºC, it exhibited the minimum j_{corr} and CR values of 0.002947 A/cm^2 and 34.240 mm/year (Fig. 2), respectively, which were lower than those of the AW sample [25]. This showed that minimal ingression of Cl$^-$ ions into the PWHT MS sample active sites occurred [26], and that it was subjected to the most favorable HT temperature.

Furthermore, Fig. 3 shows SAE 1015 PWHT and AW MS samples polarization curves (Tafel plots) of the welded sample. The figure indicates that the PWHT MS sample polarization curves shifted towards a more negative region than those from the AW one. This behavior indicates that PWHT enhanced the material cathodic polarization in the test medium.
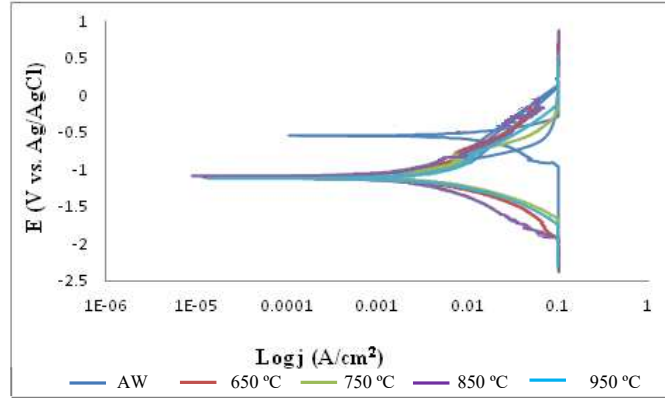
Figure 3. Polarization curves for AW and PWHT SAE 1015 MS samples, at different temperatures.

Table 4, Figs. 4 and 5 revealed the effect of simulated seawater (3.5 wt.% NaCl) on AW and PWHT SAE 1010 MS samples.

Table 4. Polarization data for AW and PWHT SAE 1010 MS samples, at different temperatures.

Temp.	E_{corr} (V)	j_{corr} (A/cm^2)	CR (mm/year)	R_p (Ω)
AW	-0.7106	0.010163	118.09	11.215
PWHT at 650 ºC	-1.1897	0.003081	35.79	24.848
PWHT at 750 ºC	-1.1933	0.003085	35.80	21.106
PWHT at 850 ºC	-1.2022	0.003461	40.22	18.435
PWHT at 950 ºC	-1.1675	0.005172	60.10	21.369
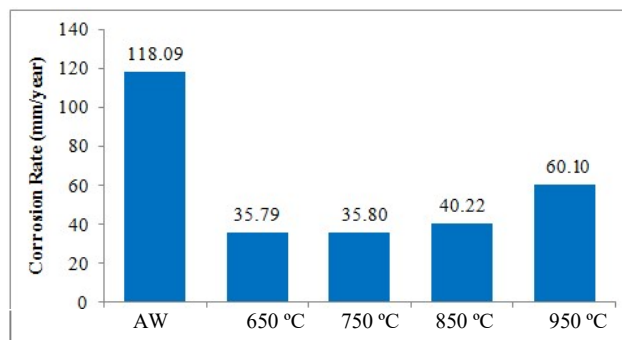
Figure 4. AW and PWHT SAE 1010 MS samples CR values.

Table 4 shows that the PWHT MS sample had lower corrosion j_{corr} values than those from the AW one. At 650 ºC, it exhibited the minimum j_{corr} value of 0.003081 A/cm^2, which could be ascribed to the HT that reduced the Cl$^-$ ions effect on the PWHT MS surface. Some proportion of passive film could have been formed on the metal surface after HT, leading to a stronger anti-corrosive property [27]. Similarly, Fig. 4 indicates

that the PWHT SAE 1010 MS sample had lower CRs values than those from the AW one, which shows that minimal penetration of Cl^- ions into the metal active sites occurred. At 650 ºC, it displayed the lowest CR of 35.79 mm/year. This reveals that the PWTH MS sample was subjected to the most favorable HT temperature, leading to a remarkable reduction in CR, compared to the AW one.

Moreover, Fig. 5 shows the AW SAE 1010 MS sample Tafel plots. The PWHT MS sample Tafel plots shifted towards a more negative region than the polarization curve from the AW one. However, the PWHT MS sample polarization curves, at 950 ºC, exhibited similar behavior as the AW one.
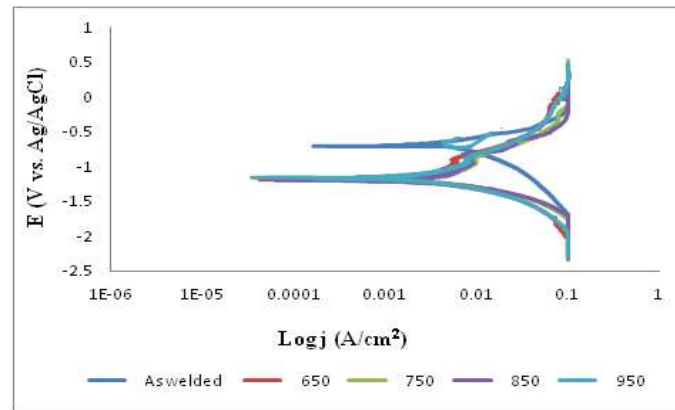
Figure 5. Polarization curves for AW and PWHT SAE 1010 MS samples.

Microstructure properties
Figs. 6 and 7 show the SEM images of PWHT SAE 1015 and 1010 MS samples, respectively, at 650 and 950 ºC. It is seen that the two PWHT MS samples, at both temperatures, exhibited a similar microstructure.
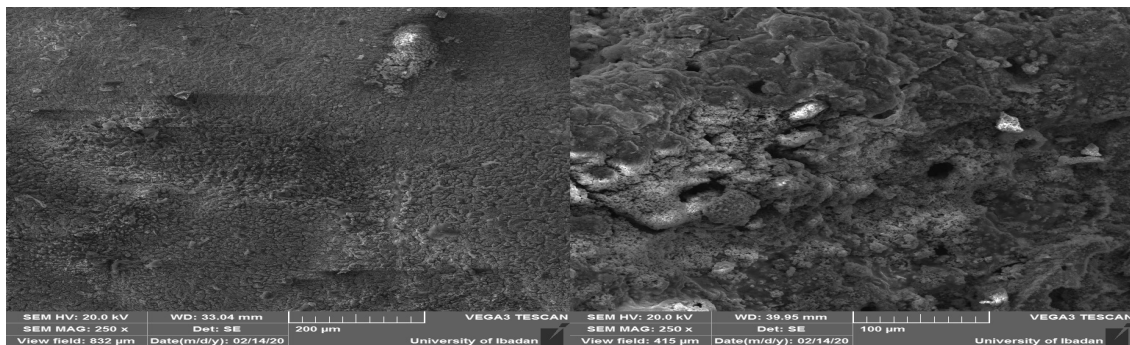
Figure 6. SEM images of PWHT SAE 1015 MS sample, at 650 and 950 ºC.

The PWHT MSs samples, at 650 ºC, exhibited lower porosity, smaller grain size and boundaries, and more uniform structures than those at 950 ºC. This behavior is in agreement with the study of Kazemipour M. et al. [28], where the metal grain size increased with higher HT temperatures.

The remarkably reduced CR and j_{corr} values observed in PWHT SAE 1015 and 1010 MS samples, at 650 ºC, could have been due to their low porosity, smaller grain size and boundaries, which minimized Cl^- ions ingression. On the contrary, their higher porosities and grain boundaries, at 950 ºC, could have acted as

crevices for corrosion initiation and propagation. Pitting corrosion attack is often predominantly on the grain boundaries, where higher lattice energy and defects exist. Therefore, the crevices acted as sites for Cl$^-$ ions strong penetration, thereby increasing the metal CR rate.
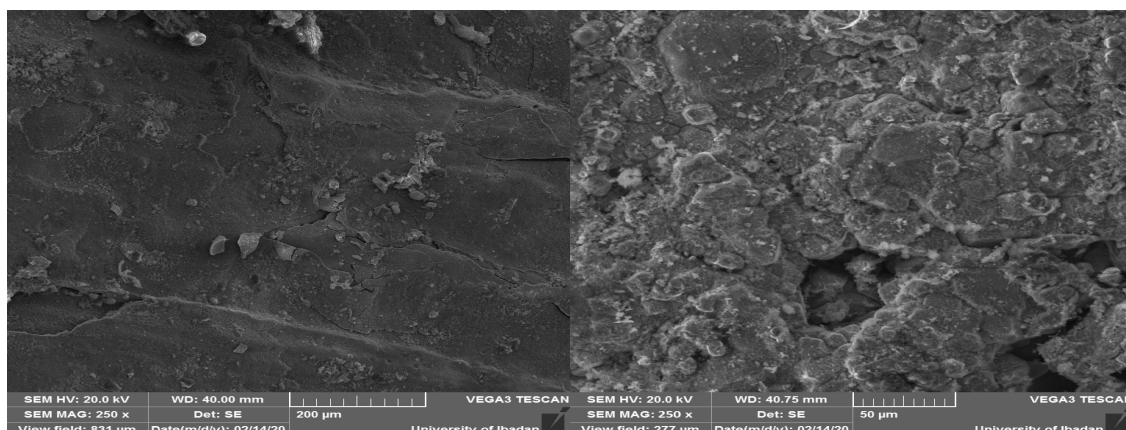
Figure 7. SEM image of PWHT SAE 1010 sample, at 650 and 950 ºC.

Conclusions

PWHT effect, by electric metal AW, on SAE 1015 and 1010 MS samples corrosion and microstructure properties was investigated, and the following conclusions were drawn:

1. The lowest CR values, of 34.240 and 35.793 mm/year, were observed for PWHT SAE 1015 and 1010 MS samples, respectively, at 650 ºC.
2. The highest CR values, of 90.16 and 60.10 mm/year, were observed for those samples, respectively, at 950 ºC.
3. For AW SAE 1015 and 1010 MS samples, the CR values were 107.54 and 118.09 mm/year, respectively.
4. The reduction in both PWHT MS samples CR values could be ascribed to the formation of passive films on their surfaces, which enhanced their corrosion resistance.
5. The SEM images, at 650 ºC, revealed smaller grain sizes and boundaries and less porosity than those at 950 ºC, which indicates that they can be utilized for advanced industrial applications.

Authors' contributions

O. O. Ajide: conceived and designed the analysis; offered key intellectual support, assessed and appraised the manuscript; developed some sections of the manuscript, revised the manuscript. **O. O. Anifalaje**: performed experiments and analyzed data; developed some sections of the manuscript. **I. G. Akande**: analyzed data; developed some sections of the manuscript; revised the manuscript. **F. A. Musa**: assisted in plagiarism test and editing of the manuscript. **O. S. I. Fayomi**: provided laboratory, offered key intellectual support, assessed, reviewed and appraised the manuscript. **O. O. Oluwole**: offered key intellectual support, assessed, reviewed and appraised the manuscript. **K. M. Oluwasegun**:

assisted in plagiarism test and editing of the manuscript. **O. J. Ajao**: reviewed and edited the manuscript.

Abbreviations
AW: as-welded
CE: counter electrode
CR: corrosion rate
CV: cyclic voltammogram
E$_{corr}$: corrosion potential
HAZ: heat-affected zone
j$_{corr}$: current density
MS: mild steel
N^3: nitrides
O^{-2}: oxides
OCP: open circuit potential
OES: optical emission spectroscopy
PDP: potentiodynamic polarization
PWHT: post-weld heat-treatment
RE: reference electrode
R$_p$: polarization resistance
SCE: saturated calomel
SEM: scanning electron microscopy
SR: scan rate
WE: working electrode

References
1. Haghdadi N, Laleh M, Moyle M et al. Additive manufacturing of steels: a review of achievements and challenges. J Mat Sci. 2021;56(1):64-107. https://doi.org/10.1007/s10853-020-05109-0
2. Sedik A, Lerari D, Salci A et al. Dardagan Fruit extract as eco-friendly corrosion inhibitor for mild steel in 1 M HCl: Electrochemical and surface morphological studies. J Taiwan Instit Chem Eng. 2020;107:189-200. https://doi.org/10.1016/j.jtice.2019.12.006
3. Fayomi OSI, Akande IG, Oluwole OO et al. Effect of water-soluble chitosan on the electrochemical corrosion behaviour of mild steel. Chem Data Coll. 2018;17:321-326. https://doi.org/10.1016/j.cdc.2018.10.006
4. Schmitt JH, Iung T. New developments of advanced high-strength steels for automotive applications. Comptes Rendus Physique. 2018;19(8):641-656. https://doi.org/10.1016/j.crhy.2018.11.004
5. Song B, Nishida E, Sanborn B et al. Compressive and tensile stress–strain responses of additively manufactured (AM) 304L stainless steel at high strain rates. J Dynam Behav Mat. 2017;3(3):412-425. https://doi.org/10.1007/s40870-017-0122-6
6. Oladele IO, Alonge DB, Betiku TO et al. Performance Evaluation of the Effects of Post Weld Heat Treatment on the Microstructure, Mechanical and Corrosion Potentials of Low Carbon Steel. Adv Technol Mat. 2019;44(2):42-46. https://10.24867/ATM-2019-1-007

7. Chung IM, Kim SH, Hemapriya V et al. Inhibition behavior of *Tragia involucrata L.* phenolic compounds against acidic medium corrosion in low carbon steel surface. Chin J Chem Eng. 2019;27(3):717-25. https://doi.org/10.1016/j.cjche.2018.10.008

8. Wang P, Ryberg M, Yang Y et al. Efficiency stagnation in global steel production urges joint supply-and demand-side mitigation efforts. Nat Communic. 2021;12(1):1-11. https://doi.org/10.1038/s41467-021-22245-6

9. Raabe D, Tasan CC, Olivetti EA. Strategies for improving the sustainability of structural metals. Nature. 2019;575(7781):64-74. https://doi.org/10.1038/s41586-019-1702-5

10. Matsui H, Hattori T. Abrasion phenomena of the contact tip in consumable electrode arc welding. Weld Int. 2018;32(7):475-484. https://doi.org/10.1080/01431161.2017.1346886

11. Hammad A, Churiaque C, Sánchez-Amaya JM et al. Experimental and numerical investigation of hybrid laser arc welding process and the influence of welding sequence on the manufacture of stiffened flat panels. J Manuf Proc. 2021;61:527-538 https://doi.org/10.1016/j.jmapro.2020.11.040

12. Yelamasetti B, Vardhan TV, Ramana GV. Study of metallurgical changes and mechanical properties of dissimilar weldments developed by interpulse current TIG welding technique. Proceedings of the Institution of Mechanical Engineers. Part C: J Mech Eng Sci. 2021;235(16):2985-2997. https://doi.org/10.1177/0954406220960780

13. Kumar B, Bag S, Mahadevan S et al. On the interaction of microstructural morphology with residual stress in fiber laser welding of austenitic stainless steel. CIRP J Manuf Sci Technol. 2021;33:158-175. https://doi.org/10.1016/j.cirpj.2021.03.009

14. Udayakumar T, Raja K, Abhijit AT et al. Experimental investigation on mechanical and metallurgical properties of super duplex stainless steel joints using friction welding process. J Manuf Proc. 2013;15(4):558-571. https://doi.org/10.1016/j.jmapro.2013.06.010

15. Ding S, Xiang S, Ba X et al. Improvement of Corrosion Resistance of Simulated Weld Heat Affected Zone in High Strength Pipeline Steel Using Electropulsing. ISIJ Int. 2020;60(9):2015-2023. https://doi.org/10.2355/isijinternational.ISIJINT-2019-565

16. Khan M, Dewan MW, Sarkar MZ. Effects of welding technique, filler metal and post-weld heat treatment on stainless steel and mild steel dissimilar welding joint. J Manuf Proc. 2021;64:1307-1321. https://doi.org/10.1016/j.jmapro.2021.02.058

17. Pankade SB, Ambad PM, Wahane R et al. Effect of the Post-weld Heat Treatments on Mechanical and Corrosion Properties of Friction Stir-Welded AA 7075-T6 Aluminium Alloy. In Strengthening and Joining by Plastic Deformation. 2019:79-94. Springer, Singapore. DOI: https://doi.org/10.1007/978-981-13-0378-4_4

18. Huang B, Liu J, Zhang S et al. Effect of post-weld heat treatment on the residual stress and deformation of $20/0Cr_{18}Ni_9$ dissimilar metal welded joint by experiments and simulations. J Mat Res Technol. 2020;9(3):6186-6200. https://doi.org/10.1016/j.jmrt.2020.04.022

19. Kashaev N, Ventzke V, Çam G. Prospects of laser beam welding and friction stir welding processes for aluminum airframe structural applications. J Manuf Proc. 2018;36:571-600. https://doi.org/10.1016/j.jmapro.2018.10.005

20. Eisazadeh H, Aidun DK. Residual stress reduction in dissimilar metals weld. J Manuf Proc. 2021;64:1462-1475. https://doi.org/10.1016/j.jmapro.2021.02.062

21. An JH, Lee J, Kim YS et al. Effects of post weld heat treatment on mechanical and electrochemical properties of welded carbon steel pipe. Met Mat Int. 2019;25(2):304-312. https://doi.org/10.1007/s12540-018-0201-9

22. Joseph GB, Valarmathi TN, Rajan AJ et al. Characteristics study of post weld heat treatment in SA 387 grade 22 steel by cladding using gas tungsten arc welding process. Mat Today: Proceed. 2021;44:3798-3802. https://doi.org/10.1016/j.matpr.2020.12.332

23. Farhadi A, Zhu Y, Gu L et al. Influence of electrode shape and size on electric arc channel and crater. Procedia Cirp. 2018;68:215-220. https://doi.org/10.1016/j.procir.2017.12.051

24. Zhu G, Zhang M, Zhang Q et al. Investigation of a single-pulse electrical arc discharge in vacuum based on the crater morphology and discharge channel. Int J Adv Manuf Technolog. 2020;107(7):3437-3448. https://doi.org/10.1007/s00170-020-05163-7

25. Ghorbani S, Ghasemi R, Ebrahimi-Kahrizsangi R et al. Effect of post weld heat treatment (PWHT) on the microstructure, mechanical properties, and corrosion resistance of dissimilar stainless steels. Mat Sci Eng: A. 2017;688:470-479. https://doi.org/10.1016/j.msea.2017.02.020

26. Akande IG, Fayomi OSI, Oluwole OO. Anticorrosion Potential of Inhibitive Suphtrim Drug on Aluminium Alloys in 0.5 M H_2SO_4. J Bio-and Tribo-Corros. 2020;6(4):1-8. https://doi.org/10.1007/s40735-020-00429-9

27. Kong D, Ni X, Dong C et al. Heat treatment effect on the microstructure and corrosion behavior of 316L stainless steel fabricated by selective laser melting for proton exchange membrane fuel cells. Electrochim Acta. 2018;276:293-303. https://doi.org/10.1016/j.electacta.2018.04.188

28. Kazemipour M, Mohammadi M, Mfoumou E et al. Microstructure and corrosion characteristics of selective laser-melted 316L stainless steel: the impact of process-induced porosities. Jom. 2019;71(9):3230-3240. https://doi.org/10.1007/s11837-019-03647-w